Influence of fog on the signal to interference plus noise ratio of the imaging laser radar using a 16-element APD array

WENHUA SONG,[1,&] JIANCHENG LAI,[1,&,*] ZABIH GHASSEMLOOY,[2,3] SHANGWEN LI,[1] PEIDE ZHANG,[1] WEI YAN,[1] CHUNYONG WANG,[1] AND ZHENHUA LI[1,*]

[1] *Information Physics and Engineering, Nanjing University of Science and Technology, Nanjing, Jiangsu, 210094, China*
[2] *Optical Communications Research Group, NCRLab, Faculty of Engineering & Environment, University of Northumbria at Newcastle, Newcastle upon Tyne, NE1 8ST, UK*
[3] *QIEM, Haixi Institutes, Chinese Academy of Sciences, Quanzhou, Fujian, 350002, China*
[&] *Authors contributed equally to this work and should be considered co-first authors*
**laijiancheng@njust.edu.cn; zhenhuali@njust.edu.cn*

Abstract: This paper investigates the signal to interference plus noise ratio (SINR) performance of the imaging laser radar (ILR) system operating at a wavelength of 905 nm using an avalanche photodiode array under the fog condition. We analysis the glow image of the light source, which is formed by the laser spot irradiated on a standard Lambertian target. Based on the proposed theoretical model, we determine the interference due to the glow inter-channel crosstalk under different fog conditions for a targeted channel. We show that, for transmission spans less than several tens of meters the interference due to glow crosstalk is higher than the fog (light to medium) induced losses. However, for a link range longer than 21 m the glow crosstalk induced interference is lower than the heavy fog induced attenuation. The proposed system performance is evaluated by developing an experimental test bed and using a dedicated indoor atmospheric chamber under homogeneously controlled fog conditions. We show that, under different fog conditions experimental results for changing SINR levels match well with the predicted data. The results shown can be used for design optimization of the ILR system when operated under fog conditions.

OCIS codes: (080.0080) Geometric optics; (140.0140) Lasers and laser optics; (010.3640) Lidar; (010.1300) Atmospheric propagation; (010.5620) Radiative transfer.

References and links

1. M. A. Albota, R. M. Heinrichs, D. G. Kocher, D. G. Fouche, B. E. Player, M. E. O'Brien, B. F. Aull, J. J. Zayhowski, J. Mooney, B. C. Willard, and R. R. Carlson, "Three-dimensional imaging laser radar with a photon-counting avalanche photodiode array and microchip laser," Appl. Opt. **41**(36), 7671-7678 (2002).
2. K. Bers, K. R. Schulz, and W. Armbruster, "Laser radar system for obstacle avoidance," in Proc. SPIE **5958**, Lasers and Appl., (2005).
3. A. Matwyschuk, "Multiple-wavelength range-gated active imaging in superimposed style for moving object tracking," Appl. Opt. **56**(27), 7766-7773 (2017).
4. M. M. Kleiman and N. Shiloah, "The effect of dense atmospheric environment on the performances of laser radar sensors used for collision avoidance," in Proc. SPIE **3707**, Laser Radar Tech. and Appl. IV, 624–635 (1999).
5. H. N. Burns, C. G. Christodoulou, and G. D. Boreman, "System design of a pulsed laser rangefinder," Opt. Eng. **30**(3), 323–329 (1991).
6. Y. Yang, M. Mandehgar, and D. Grischkowsky, "Time domain measurement of the THz refractivity of water vapor," Optics express **20**(24), 26208–26218 (2012).
7. Y. Yang, M. Mandehgar, and D. Grischkowsky, "Broadband THz signals propagate through dense fog," IEEE Photonics Technology Letters **27**(4), 383–386 (2015).
8. Z. Ghassemlooy, W. Popoola, and S. Rajbhandari, *Optical Wireless Communications – System and Channel Modelling with Matlab* (CRC publisher, 2012).
9. M. Grabner and V. Kvicera, "The wavelength dependent model of extinction in fog and haze for free space optical communication," Opt. Exp. **19**(4), 3379–3386 (2011).

10. M. Ijaz, Z. Ghassemlooy, J. Pesek, O. Fiser, H. L. Minh, and E. Bentley, "Modeling of Fog and Smoke Attenuation in Free Space Optical Communications Link Under Controlled Laboratory Conditions," J. Lightw. Technol. **31**(11), 1720–1726 (2013).
11. M. A. Naboulsi, H. Sizun, and F. Fornel, "Fog attenuation prediction for optical and infrared waves," Opt. Eng. **43**(2), 319–329 (2004).
12. M. Grabner and V. Kvicera, "Multiple scattering in rain and fog on Free-Space-Optical links," J. Lightw. Technol. **32**(3), 513–520 (2014).
13. R. Nebuloni, "Empirical relationships between extinction coefficient and visibility in fog," Appl. Opt. **44**(18), 3795–3804 (2005).
14. M. Uysal, C. Capsoni, Z. Ghassemlooy, A. C. Boucouvalas, and E. G. Udvary (Eds.), *Optical Wireless Communications – An Emerging Technology* (Springer, 2016).
15. C. Niclass, K. Ito, M. Soga, H. Matsubara, I. Aoyagi, S. Kato, and M. Kagami, "Design and characterization of a 256x64-pixel single-photon imager in CMOS for a MEMS-based laser scanning time-of-flight sensor," Opt. Express **20**(11), 11863-11881 (2012).
16. G. Kim and Y. Park, "LIDAR pulse coding for high resolution range imaging at improved refresh rate," Opt. Express **24**(21), 23810-23828 (2016).
17. M. A. Albota, R. M. Heinrichs, D. G. Kocher, D. G. Fouche, B. E. Player, M. E. O'Brien, B. F. Aull, J. J. Zayhowski, J. Mooney, B. C. Willard, and R. R. Carlson, "Three-dimensional imaging laser radar with a photon-counting avalanche photodiode array and microchip laser," Appl. Opt. **41**(36), 7671-7678 (2002).
18. J. D. Klett, "Lidar inversion with variable backscatter/extinction ratios," Appl. Opt. **24**(11), 1638-1643 (1985).
19. S. G. Narasimhan, and S. K. Nayar, "Shedding light on the weather," in Proceedings of the IEEE Computer Society Conference on Computer Vision and Pattern Recognition (Institute of Electrical and Electronics Engineers, Madison, Wisconsin, 2003) 665-672.
20. P. Djahani and J. M. Kahn, "Analysis of infrared wireless links employing multi-beam transmitters and imaging diversity receivers," IEEE Transactions on Communications **48**(12), 2077-2088 (2000).
21. F. Taillade1, E. Belin, and E. Dumont, "An analytical model for backscattered luminance in fog: comparisons with Monte Carlo computations and experimental results," Meas. Sci. Tech. **19**(5), 055302-055309 (2008).
22. J. W. Giles, I. N. Bankman, R. M. Sova, T. R. Morgan, D. D. Duncan, J. A. Millard, W. J. Green, and F. J. Marcotte, "Lidar system model for use with path obscurants and experimental validation," Appl. Opt. **47**(22), 4085-4093 (2008).
23. W. Song, J. Lai, Z. Ghassemlooy, Z. Gu, W. Yan, C. Wang, Z. Li, "The effect of fog on the probability density distribution of the ranging data of imaging laser radar," AIP Advances **8**(2), 025022 (2018).
24. H. C. van de Hulst, "Light Scattering by Small Particles," Dover Publications, New York, 1981.
25. S. Mori and F. S. Marzano, "Microphysical characterization of free spaceoptical link due to hydrometeor and fog effects," Appl. Opt. **54**(22), 6787-6803 (2015).
26. C. F. Bohren, D. R. Huffman, "Absorption and scattering of light by small particles," John Wiley & Sons, 2008.
27. I. I. Kim, B. McArthur, and E. J. Korevaar, "Comparison of laser beam propagation at 785 nm and 1550 nm in fog and haze for optical wireless communications," Proc. SPIE **4214**, 26–37 (2001).
28. P. Corrigan, R. Martini, E. A. Whittaker, and C. Bethea, "Quantum cascade lasers and the Kruse model in free space optical communication," Opt. Express **17**(6), 4355–4359 (2009).
29. M. Ijaz, Z. Ghassemlooy, S. Rajbhandari, H. L. Minh, J. Perez, and A. Gholami, "Comparison of 830 nm and 1550 nm based free space optical communications link under controlled fog conditions," IEEE 8th CSNDSP Int. Symposium, 2012.
30. R. G. Eldridge, "Haze and fog aerosol distributions," J. Atmos. Sci. **23**(5), 605–613 (1966).
31. J. Redemann, R. P. Turco, K. N. Liou, P. B. Russell, R. W. Bergstrom, B. Schmid, J. M. Livingston, P. V. Hobbs, W. S. Hartley, S. Ismail, R. A. Ferrare, E. V. Browell, "Retrieving the vertical structure of the effective aerosol complex index of refraction from a combination of aerosol in situ and remote sensing measurements during TARFOX," J. Geo. Res. **105**(8), 9949-9970 (2000).
32. R. M. Measures, *Laser Remote Sensing: fundamentals and applications* (Krieger, 1992).
33. L. C. Andrews, and R. L. Phillips, *Laser beam propagation through random media* (Bellingham, WA: SPIE press, 2005).
34. A. Ishimaru, *Wave propagation and scattering in random media* (Academic Press, 1978).
35. S. Chandrasekhar, *Radiative transfer* (Dover Publications, 1960).
36. R. N. Mahalati and J. M. Kahn, "Effect of fog on free-space optical links employing imaging receivers," Opt. Express **20**(2), 1649-1661 (2012)
37. E. Gramsch. "Noise Characteristics of Avalanche Photodiode Arrays of the Bevel-Edge Type," IEEE Transactions on Electron Devices **45**(7), 1587-1594 (1998).
38. H. T. Eyyuboğlu and M. Bayraktar, "SNR bounds of FSO links and its evaluation for selected beams," Journal of Modern Optics **62**(16), 1316-1322 (2015).
39. V. Rajamani, P. Chakrabarti. "Noise Performance of an InP/InGaAs Superlattice Avalanche Photodiode," Optical and Quantum Electronics **31**(1), 69-76 (1999).
40. W. Song, Z. Ghassemlooy, J. Lai, Wei Yan, C. Wang, Z. Li. "The irradiating field of view of imaging laser radar under fog conditions in a controlled laboratory environment," Journal of Optics **19**(4), 045605 (2017).

1. Introduction

Over the past few decades, imaging laser radar (ILR) systems with high-resolution three-dimensional (3-D) images [1] have become an attractive option for range finding in a number of applications including target recognition, object imaging, obstacle avoidance to name a few [2–5]. However, in line with any free space optical (FSO) transmission in outdoor environments the performances of ILR system is highly dependent on the weather conditions (i.e., fog, rain, snow, pollution, sand storms, and turbulence), which has been investigated widely [8, 14]. Among these, fog is the most troublesome in terms of optical attenuation where losses as high as 480 dB/km and 120 dB/km for dense maritime and moderate continental fog conditions, respectively have been reported with the consequences of drastically reduced link visibility to less than 100 meters [6, 7]. For more on fog and the models developed for FSO system the readers are referred to [8-14]. Most studies reported on the FSO links have focused on the atmospheric environment induced attenuation. However, in ILR system there is an additional interference due to the glow crosstalk, which can be higher than the fog induced loss over longer transmission spans.

In ILR systems two design schemes have been widely adopted. (*i*) A laser radar with a single element based transmitter (Tx) and receiver (Rx) as well as a dual galvanometer scanning system or Micro-electromechanical Systems (MEMS), which was adopted to obtain an imaging of the scanned objects [15-18]. However, in this scheme the imaging rate is usually less than 10 Hz for a high pixel resolution. (*ii*) Multiple Txs and Rxs [17, 18], where each Tx and Rx contains of a number of semiconductor laser diode (LD) array and an avalanche photodiode (APD) array, respectively. This option offers higher imaging rate and has been widely used and therefore is adopted in this work.

The performance of the ILR system is effected under the fog condition in the form of signal attenuation due to the absorption and scattering of photons by fog droplets, the glow inter-channel crosstalk and the ambient noise. In [18] a new formulation to solve the single-scattering lidar equation was proposed by assuming that the power law relation between the backscatter and the extinction with a variable exponent as well as the proportionality factor being a function of the range or the extinction. The resulting lidar equation provided an improved inversion solution for the extinction. In [19] an analytical model for multiple scattering of light traversing through the atmosphere was presented showing how the shape of the glow was related to the visibility and conditions of the atmospheric channel as well as the depth and shape of the light source. The model could be used for real-time rendering of sources under different atmospheric conditions. In [20] improvements obtained in wireless infrared (IR) communication links were analyzed by replacing the traditional single-element Rxs with the imaging Rxs and the diffuse Txs with the multi-beam (quasi-diffuse) Txs for both line-of-sight (LOS) and non-line-of-sight (non-LOS) IR links. The results showed that in LOS links the imaging Rxs can reduce the required transmit power by up to 13 dB compared to single-element Rxs, whereas in non-LOS links with the imaging Rxs and multi-beam Txs the required transmit power was reduced by more than 20 dB. However, to the best of our knowledge no works on the influence of the glow crosstalk experienced in ILR system under different fog conditions have been reported yet.

In this paper, we presented a theoretical model to calculate the glow image of the light source, which is formed by the laser spot irradiated on a standard Lambertian target. Based on the proposed theoretical model, we determine the level of interference due to the glow crosstalk and assess the link performance accordingly. In addition, we investigate the channel loss and glow crosstalk for different fog densities and show that for a link span less than several tens of meters the glow crosstalk induced interference is always large than the fog (light to medium) imposed attenuation. Only under the heavy fog condition does the attenuation exceed the glow crosstalk loss when the ranging distance longer than ~21 m. In order to verify the accuracy of the theoretical model, we developed an experimental setup for evaluating the effect of fog on the 12 channels of the proposed ILR system. We show that the experimental results for SINR of all channels under different fog conditions matched well with the predicted data. The results

reported can be used to optimize the design of the ILR system and analyzing its performance in the presence of fog influences.

The rest of this paper is organized as follows: section 2 describes details of the light propagation through fog while section 3 focuses on the influence of fog on the 12 channels of the ILR system theoretically and experimentally. Section 4 is the discussion of the limitations of our model. Finally, the concluding remarks are presented in Section 5.

2. Light propagation through fog

In an outdoor environment the distribution of fog droplets, which can change very rapidly in both space and time, is the most crucial in determining the channel loss in optical wireless-based systems including ILR. However, it is not straight forward to quantify the distribution of fog droplet sizes due to the influence of different physical processes, thus the introduction of a number of drop size distribution (DSD) based models. One of the classical and widely used model is the lognormal distribution, which is given by [12, 19, 21-24]:

$$n(r) = \frac{N_0}{\sqrt{2\pi}\sigma_r r} \exp\left[-\frac{1}{2}\left(\frac{\ln(r) - \mu_r}{\sigma_r} \right)^2 \right], \tag{1}$$

where N_0 is the particle number density, r is the particle size radius, and μ_r and σ_r are logarithmic mean value and standard deviation of particle radius, respectively.

The exact DSD model of fog can be determined by knowing the values of μ_r and σ_r, however, due to the complex physical properties of fog its distribution is not readily available. Thus the effective radius of distribution r_e and the liquid water content (*LWC*) are used for characterization of fog, which are proportional to the total volume of particles, see [23, 25] for more details.

For the fog particle sizes being in the order of the propagating light (in this case laser) wavelength λ, Mie theory has been used as in [23, 24] with the extinction coefficient being defined by [26, 27]:

$$\sigma_{ext} = \int_0^\infty C_{ext}\left(\frac{2\pi r}{\lambda}, n'\right) n(r) dr, \tag{2}$$

where *n'* is the real part of the refractive index of water, and C_{ext} is the droplet extinction cross section. However, C_{ext} weighted by DSD is not easy to be estimated. Note that, the total extinction due to fog particles in the atmosphere is the sum of absorption and scattering of light. For λ of 905 nm, which is adopted in the proposed ILR system, the molecular absorption is considered to be negligible. Therefore, for the laser pulse the extinction coefficient can be fully estimated by the scattering cross section C_{sca} of fog as given by:

$$\sigma_{ext} = \sigma_{sca} = \int_0^\infty C_{sca}\left(\frac{2\pi r}{\lambda}, n'\right) n(r) dr, \tag{3}$$

Generally, due to the complex physical properties of fog its real time distribution and scattering cross section are not readily available. Therefore, in order to predict the fog induced attenuation, a simple empirical model has been adopted, which is given by [28, 29]:

$$\sigma_{ext}(\lambda) = \frac{3.912}{V}\left(\frac{\lambda}{0.55} \right)^{-p}, \tag{4}$$

where *V* is the link visibility, which is evaluated at 550 nm, and *p* is the exponent, which determined theoretically and experimentally research as in [30-33].

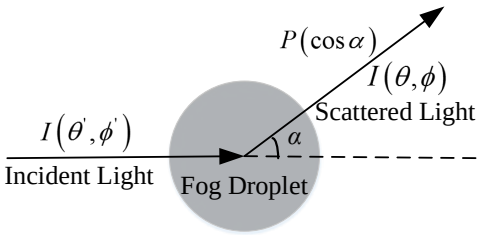

Fig. 1 The schematic diagram of the incident light scattered by a fog droplet at an angle α.

A laser beam propagating through a channel with fog (i.e., water droplets) will undergo scattering in multiple directions as shown in Fig. 1. The angular distribution of the intensity of scattered light by article suspended in the channel is best characterized by the phase function, which is given by [22]:

$$P(\cos\alpha) = P(\theta,\phi;\theta',\phi') = \frac{I(\theta,\phi)}{I(\theta',\phi')}, \tag{5}$$

where $I(\theta',\phi')$ and $I(\theta,\phi)$ are the intensities of the incident and scattered light beams along the observed direction in the spherical coordinate, respectively. For most atmospheric conditions, the phase function is usually symmetric about the incident light direction and is only a function of the scattered angle α. Using the spherical geometry the cosine of α can be expressed as:

$$\cos\alpha = \cos\theta\cos\theta' + \sin\theta\sin\theta'\cos(\phi-\phi'), \tag{6}$$

For a given size of fog droplet, the exact shape of the phase function can be determined accurately by Mie theory. However, the scattering phase function of a group of particles (i.e., fog or cloud) should be characterized by the DSD, which can be expressed as:

$$P(\cos\alpha) = \frac{\int_{r_1}^{r_2} P(\cos\alpha, r) C_{sca} n(r)\, dr}{\int_{r_1}^{r_2} C_{sca} n(r)\, dr}, \tag{7}$$

It has been shown that Henyey-Greenstein phase function is valid for a range of particles sizes and for different media, as given by [31, 32]:

$$P(\cos\alpha) = \frac{1-q^2}{(1+q^2-2q\cos\alpha)^{3/2}}, \tag{8}$$

where q, the forward scattering parameter, which is inversely proportional to the density of the medium and is within the range of [0,1] generating phase functions for different types of weather conditions. For Isotropic or Rayleigh scattering of small size particle (e.g., air molecules) q = 0, which represents light being scattered almost equally in all directions. However, for q = 1, the light is considered to be scattered in the forward direction as is the case for large size particles (e.g., light to heavy fog). Note that, eq. (8) is not normalized and therefore can integral over the 4π steradian to make it unity.

The changes in light radiance propagating through a dispersion medium at each direction for every points in space can be governed by the radiative transfer equation (RTE), where its differential form is defined as [33, 34]:

$$\mu\frac{\partial I}{\partial T} + \frac{1-\mu^2}{T}\frac{\partial I}{\partial \mu} = -I(T,\mu) + \frac{1}{4\pi}\int_0^{2\pi}\int_{-1}^{1} P(\cos\alpha) I(T,\mu')\, d\mu' d\phi', \tag{9}$$

where $\mu = \cos\theta$, $\mu' = \cos\theta'$, I is the radiance of light, and $T = \sigma_{ext} l$ is the optical thickness a dimensionless quantity, which determines the amount attenuation experienced by the light propagating through the channel of range l from the viewer due to the scattering particles. Therefore, multiple scattering of light when propagation through a medium with scattering particles can be described by three parameters of T, the phase function of the particles and q. However, for a general phase function, there is no analytical solution for RTE and can be conjectured to be non-existent to some extent. Narasimhan and Nayar [19] showed that, a series solution to the RTE for an isotropic point source can be obtained by expanding Henyey-Greenstein phase function in terms of Legendre polynomials, which is given as:

$$I(T,\mu) = I_0 \sum_{n=0}^{\infty} \left[g_n(T) + g_{n+1}(T) \right] L_n(\mu), \tag{10}$$

where $I(T,\mu)$ is the intensity of the light at the observation point, I_0 is the radiance of the isotropic point source, $L_n(\mu)$ is the Legendre polynomial of order n, and the series $g_n(T)$ is defined as:

$$g_n(T) = \begin{cases} 0 & n = 0 \\ \exp\left[-(n+1)\ln T - \dfrac{2n+1}{n}\left(1 - q^{n-1}\right) T \right] & n \neq 0 \end{cases}, \tag{11}$$

By combining eq. (10) and eq. (11), $g_n(T)$ represents the attenuation of light under the weather condition and L_n is expressed as the angular spread of the light in the received plane duo to multiple scattering.

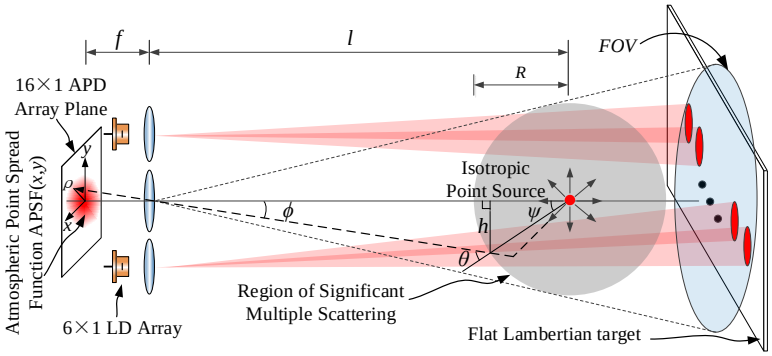

Fig. 2 Schematic diagram of 12 channels-based laser radar showing multiple scattering of the propagating beam for large remission distances and small fields of view.

Fig. 2 depicts the schematic diagram of 12 channels-based laser radar showing multiple scattering of the propagating beam for large remission distances and small fields of view. Each Tx consists of a 6×1 semiconductor laser diode (LD) array and a lens for compressing the output divergence angle, whereas the Rx is composed of a lens and a 16×1 APD array. Note, the special lenses are used to ensure that the 12 laser spots are projected on the center of 12 optical Rxs. Multiple scattering of light while propagating through the atmosphere results in the image of a point source spreading out into a spot known as the atmospheric point spread function. Note that, in an outdoor environment and using a single point light source (i.e., isotropic) the propagating beam experience random multiple scattering that results in a glow around the light source in the image plane. For a vehicle-mounted ILR system, the range distance is usually several meters to hundreds of meters and the field of view of the Rx is tens of milliradian. In this case, one can assume that the multiple scattering of light takes place only inside a sphere

surrounding the source and is within the FOV of the Rx [35]. As show in Fig. 2, the sphere represents a region of significant multiple scattering of luminous rays, whereas the area surrounding the sphere is simply modeled as the path loss. Note that, the atmospheric point spread function (APSF) is defined as an image of a point source with a unit radiant intensity obtained in an imaging system under a given atmospheric condition. The key point is to find a map between the image plane (x, y) and the variable (T, μ), and working out the relationship between the variable $\rho = \sqrt{x^2 + y^2}$ and the azimuthal angle θ. The derivation based on the geometry is given as follows:

$$
\begin{aligned}
R &= l \sin\left(\frac{FOV}{2}\right) \\
h &= \frac{\rho l f - \rho\sqrt{f^2R^2 + \rho^2 l^2 - \rho^2 R^2}}{\rho^2 + f^2} \\
\mu(\rho) &= \cos\left[\sin^{-1}\left(\frac{h}{R}\right) + \tan^{-1}\left(\frac{\rho}{f}\right)\right] \\
APSF(\rho) &= \frac{I\left[T, \mu(\rho)\right]}{I_0}\frac{\kappa}{l^2}\exp\left(-\sigma_{ext} l\right)
\end{aligned}
\quad , \tag{12}
$$

where R is the radius of the significant multiple scattering region, l is the distance between the isotropic point source and the Rx, f is the focal length of the lens at the Rx and κ is the proportional constant, which is related to the geometry of the ILR system.

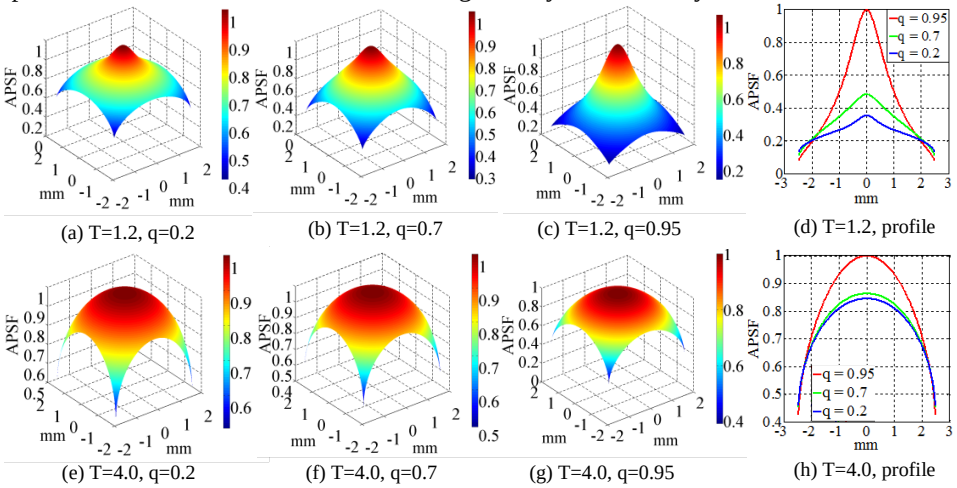

(a) T=1.2, q=0.2 (b) T=1.2, q=0.7 (c) T=1.2, q=0.95 (d) T=1.2, profile

(e) T=4.0, q=0.2 (f) T=4.0, q=0.7 (g) T=4.0, q=0.95 (h) T=4.0, profile

Fig. 3 The normalized APSF on the image plane for a low dense weather condition with T = 1.2 and a high dense weather condition with T = 4.0. Note, (d) and (h) are the cross section profiles of the corresponding APSF, respectively.

Fig. 3 shows the normalized three dimensional APSF on image plane for the ILR system for different weather conditions. The focal length and the FOV of the Rx are 50 mm and 100 mrad, respectively. The full width at half maximum (FWHM) of the APSF represents the scattering of light due to the various weather conditions. As can be seen in Fig. 3(d), for a low dense weather condition with T = 1.2 the FWHM of the APSF strongly depends on the forward scattering parameter q. The narrower FWHM due to larger q represents the light being focused more on the image plane, which indicates that fog will produce narrower glows when compared to small size aerosol particles. However, for higher dense weather conditions with T = 4.0 as shown in Fig. 3(h), FWHM is almost the same for all three values of q and is independent of

the forward scattering parameter, thus demonstrating that the glows are similar for different atmosphere conditions due to different types of scattering aerosols.

Note that, for a given atmospheric condition and assuming an isotropic light source the obtained APSF for an imaging system can be used to determine the glows of an image of any light source $I_0(x,y)$ with arbitrary shapes and sizes using a two dimensional convolution, which is given by:

$$\begin{aligned} I(x,y) &= I_0(x,y) * APSF(x,y) \\ &= \int_{-\infty}^{+\infty}\int_{-\infty}^{+\infty} I_0(x_\tau, y_\tau) APSF(x-x_\tau, y-y_\tau) dx_\tau dy_\tau \end{aligned}, \tag{13}$$

Note that, we assume that the derivation outlined here is also valid for the proposed ILR system, given as that the target used is a standard Lambertian reflector and therefore the laser spot on the target can be considered as a first order Lambertian source where any points of the laser spot behave almost like an isotropic source.

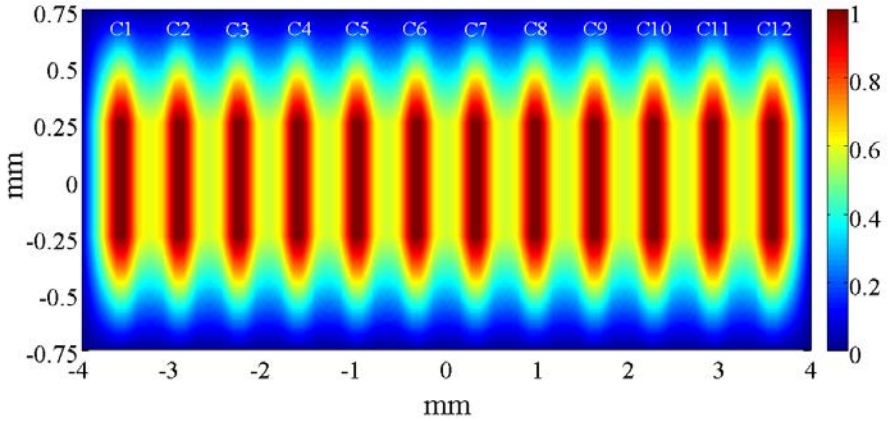

Fig. 4 The simulated result of the 12 channels glows images of the light source with a rectangular shape. The forward scattering parameter *q* and the optical thickness *T* are 0.9 and 1.2, which can be represented as the light fog conditions, respectively.

Fig. 4 shows the simulated result of the 12 channels glows images of the light source with a rectangular shape. The size of the glow of the light source $I_0(x,y)$ with a unit power is $0.4\times1.0\ mm^2$ which is corresponds to the photo-sensitive area of the APD. The light scattered by Lambertain target and then received by the Rx can be considered as incoherent superposition as displayed in Fig. 4, where under a light fog condition $I_0(x,y)$ is larger than the photo-sensitive area of the APD and therefore illuminating the next channel (i.e., crosstalk). In the next section, we will discuss the effect of fog on all 12 channels of the proposed ILR system.

3. ILR system performance under the fog condition

3.1 The experimental setup

Operating the ILR system under a normal environment condition, the SNR is an important parameter to evaluate the performance of the ILR system. For the proposed ILR system that employ an APD array, the dominant sources of noise are shot noise, thermal noise and the ambient light noise [37-39]. The shot noise is due to the signal current and the photodiode dark current, and its mean-square value is given as:

$$\sigma_{SN}^2 = 2e\left[M_f R_f P_r(l) + i_D\right] B_{PW}, \tag{14}$$

where e is the electron charge, M_f and R_f are the multiplication factor and the responsivity of the photodiode, respectively. $P_r(l)$ is the received signal power, i_D is the dark current, and B_{PW} is the electrical bandwidth of the APD. The mean-square value of the thermal noise is given by:

$$\sigma_{TN}^2 = 4k_B T_K B_{SW} F_N / R_Y \,, \tag{15}$$

where, k_B is the Boltzmann's constant, T_K is the temperature in Kelvin degrees, B_{SW} is the optimal signal bandwidth of the receiver which is related to the width of the laser pulse, F_N is the noise factor, and R_Y is the load resistor. The ambient light noise mainly due to the Sun and is defined as:

$$\sigma_{BN}^2 = 4ei_B B_{PW} \,, \tag{16}$$

where i_B is the whole ambient light induced current.

Therefore, the link SNR is defined by:

$$SNR = 10\log_{10}\left(\frac{M_f^2 R_f^2 P_r^2(l)}{2e\left[M_f R_f P_r(l) + i_D\right]B_{PW} + 4k_B T_K B_{SW} F_N / R_Y + 4ei_B B_{PW}}\right), \tag{17}$$

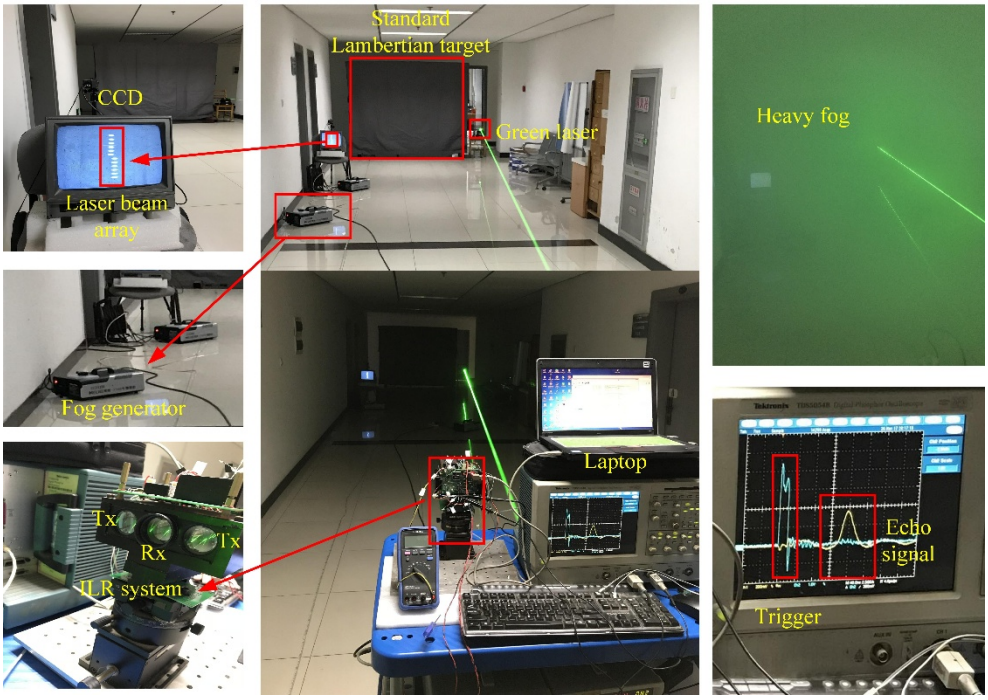

Fig. 5 The experimental setup of the proposed ILR system for testing the effect of fog on the 12 channels. In ILR system the Rx is between two Txs.

Fig. 5 shows the experimental setup for testing and evaluating the proposed system under the fog condition. The ILR system is composed of 2 optical Txs each with a 6×1 semiconductor LD array, an optical Rx with a 16×1 APD array and a free space channel. The angles of horizontal and vertical divergences of each laser spot are 5 mrad and 2 mrad, respectively. We have used a 42 long corridor as the free space channel. Fog was generated using 2 commercial

water vaporizing machines and its density and movement were controlled using two large fans positioned along the channel. The output of the Rx, composed of 12 trans-conductance amplifiers, was captured using a digital oscilloscope (Tektronix TDS5054B) for offline processing using the LABVIEW. A green laser at a wavelength λ of 532 nm and an optical power meter were used to measure the link visibility V in order to determine the fog density and the link measured fog induced attenuation. We also used a CCD camera to capture and display the laser beam array on the target. Note that, to ensure the homogeneity of fog during the entire experimental investigation a dense fog was injected into the chamber which resulted in zero visibility and then waited for the fog to become less dense. The controlled indoor medium allows us to simultaneously carry out measurements on a number transmission channels under the same fog conditions. In order to ensure reliability, repeatability and consistency of the results, each experiment was conducted five times. The key system parameters adopted in this work are given in Table. 1.

Table 1. The system structural parameters of the experiment laser radar

System	Parameter	Value
Tx	Wavelength λ	905 nm
	Pulse peak power	70 W
	Transmitting efficiency	85 %
	Pulse width (FWHM)	20 ns
	Repetition frequency	10 KHz
	Horizontal irradiating FOV	5 mrad
	Vertical irradiating FOV	2 mrad
target	Hemispherical reflectivity	75.75 %
channel	length	42 m
	width	3.5 m
	height	2.4 m
Rx	Receiver aperture diameter	0.02 m
	Receiving efficiency	90 %
	Trans-conductance	10 kΩ
	Amplifier bandwidth	50 MHz
	Receiver FOV	100 mrad
	Filter bandwidth	20 nm
	Photodetector responsivity	0.6 A/W
	Size of the photosensitive unit	0.4×1.0 mm^2
	APD reversed biased voltage	250.2 V

We measured the SNR of all 12 channels with all the lights along the corridor turned off as shown in Fig. 6. Note, in the experimental setup, we used the same voltage level of 90 V for the semiconductor laser diode (LD) array. However, the lasers have different output power levels due to their different electro-optical efficiencies. For the APD array the drive voltage level used was 152 V. Using the same LD we measure the photocurrent for each APD, which were almost the same values. Therefore, for the ILR system the observed variation in the SNR within the range of 26 - 31 dB with no fog is mainly due to LDs having different characteristic (i.e., different electro-optical efficiency).

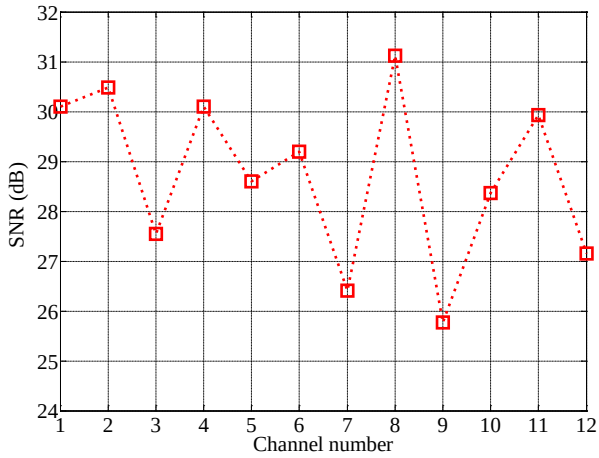

Fig. 6 The SNR of each channel with no fog which powered by 90 V and the distance between the target and the ILR system is 15 m.

However, for the ILR system operating under the fog environment, the interference due to the glow inter-channel crosstalk can be significant, see section 2, therefore, must be considered. Thus, the SINR, which is used to evaluate the performance of the ILR system under different fog conditions, is given as:

$$SINR(c_i) = 10\log_{10}\left(\frac{M_f^2 R_f^2 P_r^2(l)}{2e\left[M_f R_f P_r(l) + i_D\right]B_{PW} + 4k_B T_K B_{SW} F_N / R_Y + 4ei_B B_{PW} + M_f^2 R_f^2 (\sum_{j\neq i} P_{c_j})^2}\right) \quad (18)$$

where $\sum_{j\neq i} P_{c_j}$ is the sum of the interference power (from all the other interfering channel signals).

3.2 Analysis and results

(a) *The link performance with fog*: Considering the rotational symmetry of the channels of the ILR system, we selected the channels 1 (c1) and 6 (c6) to investigate the SINR under different fog conditions. The c1 represents the edge element of the APD array, which will be affected only by one side channels, whereas, c6 is influenced by almost all the channels depending of course on the fog density.

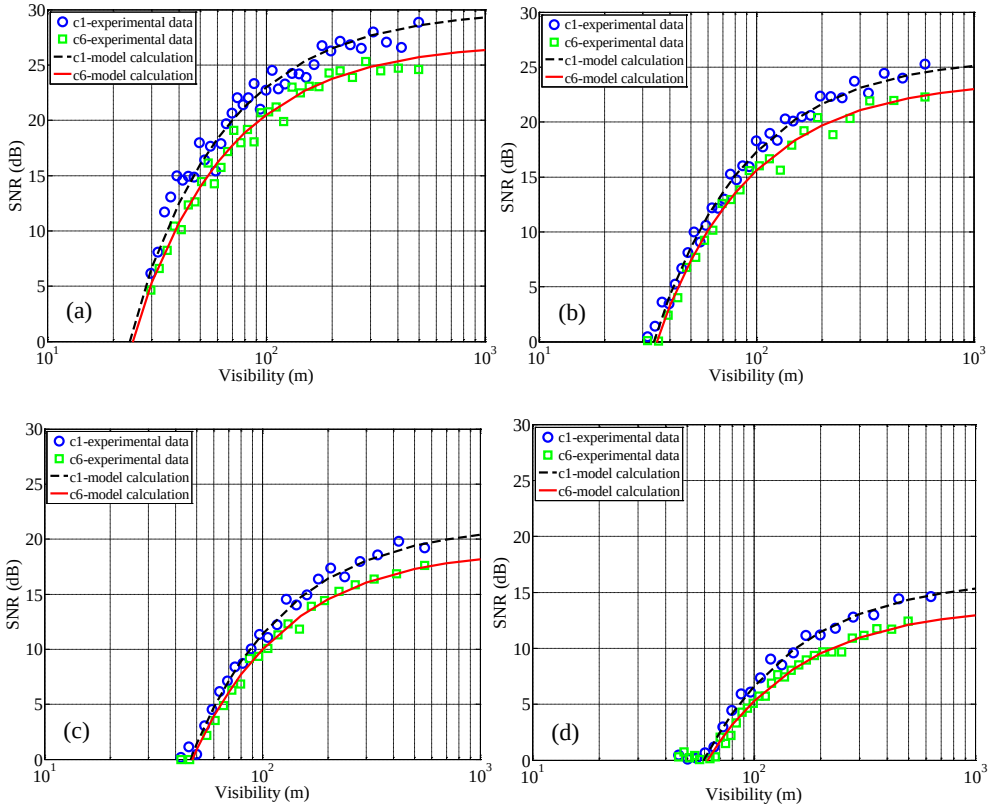

Fig. 7 The SINR of channels 1 and 6 for different visibilities and the distance between the target and the ILR system of: (a) 15 m, (b) 20 m, (c) 25 m, and (d) 30m.

Fig. 7 depicts the measured and predicted SINR of the received signal for channels 1 and 6 as a function of the link visibility for the ILR system and for a range of distances between the target and the ILR system and the parameters given in Table. 1, which shows a good match between the measured and predicted results. AS shown the SINR improved with the visibility but drops with the link span (as expected) with the channel 1 displaying improved SINR performance compared to the channel 6. E.g., at a visibility of 1000 m the SINR for the channel 1 are between 2 and 3 dB compared with the Channel 6. This improvement are mainly due to (*i*) the original SINR of the channel 1 with no fog is ~1 dB higher than channel 6; and (*ii*) the crosstalk induced by the inter-channel and increased image size of the received signal.

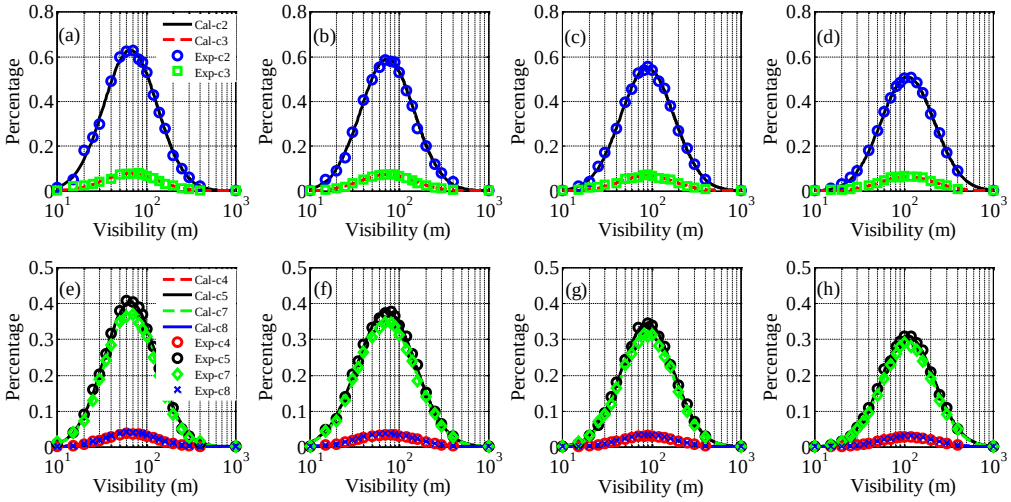

Fig.8 The inter-channel crosstalk (%) against the visibility for a range of the distances between the target and the ILR system of (a&e) 15 m, (b&f) 20 m, (c&g) 25 m and (d&h) 30 m, for: (a)-(d) channel 1, and (e)-(h) channel 6.

Fig. 8 illustrates the inter-channel crosstalk as a function of the link visibility for a range of the distances between the target and the ILR system of ((a&e) 15 m, (b&f) 20 m, (c&g) 25 m and (d&h) 30m for: (a)-(d) channel 1, and (e)-(h) channel 6 showing a good match between the experimental and theoretical results. As can be seen in Figs. 8(a)-(d) that, the channel 1 is only effected by lights from channels 2 (c2) and 3 (c3) and with no contributions from other channels. Note that, the cross talk for both channels have the same profile with c2 displaying a much higher level of crosstalk, which increases rapidly with visibility below 100 m reaching a peak value at the visibility of 60-70 m and dropping at the visibility of > 70 m. Figs. 8(e)-(h) represent the crosstalk c6 due to channels 4, 5, 7 and 8, with c5 and c7 having the most contributions. Note that the followings: (*i*) the slight difference in the level of crosstalk due to the c5 and c7 is mainly due to the initial laser transmit power, see Fig. 6; and (*ii*) the drop in the peak value of the crosstalk with the increase in the visibility distance (i.e., higher path loss).

(b) The link performance considering the laser spot duty cycle: The angles of horizontal and vertical divergences of each laser spot were controlled using a special lens. Figure 9 depicts the captured laser spots on the target where the d_{spot} and d_{duty} are shown. Note that, the real output laser beam array of the ILR system is shown in Fig. 5.

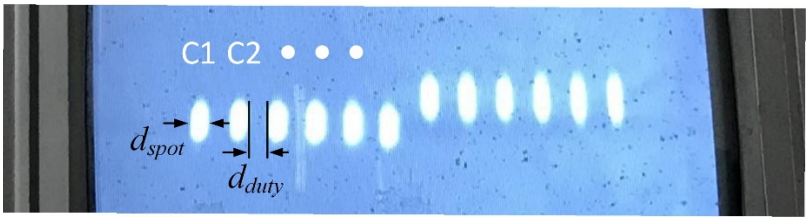

Fig. 9 The captured laser spots on the target.

By adjusting the parameters of the optical lens, the size and the position of the spot on the target can be accurately controlled, which will affect the SINR of the ILR system under different fog conditions. Here, the laser spot duty factor is defined to express the different size and the position of the spot on the target, which is given by:

$$\eta_{df} = \frac{d_{spot}}{d_{duty}} \times 100\%, \tag{19}$$

where d_{spot} is the size of the laser spot along the array direction, and d_{duty} is the interspace between the two adjacent laser spot.

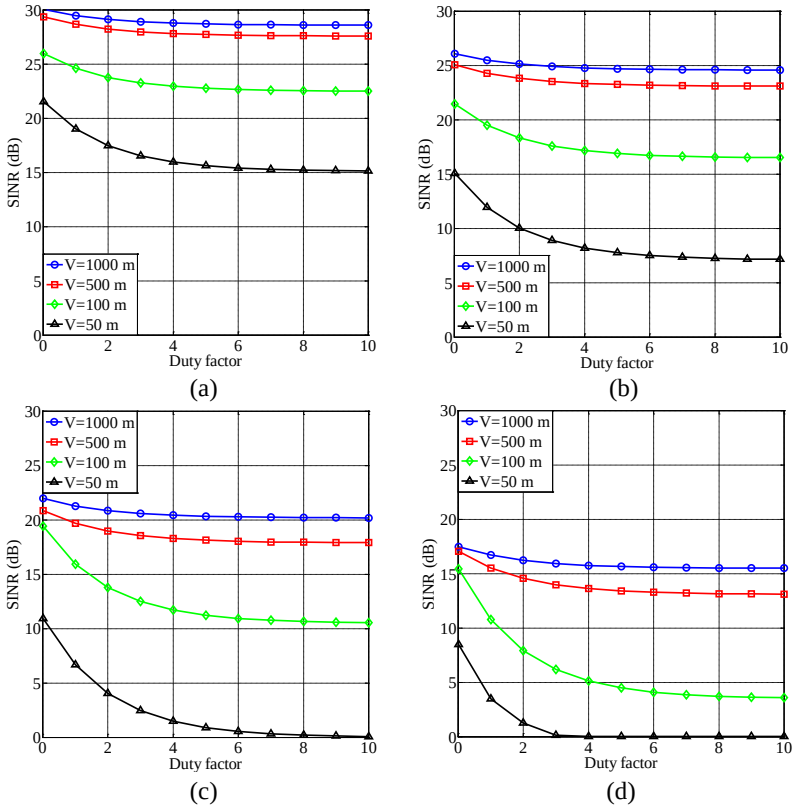

Fig. 10 The SINR change of channel 1 as a function of the laser spot duty factor under different visibilities and the distance between the target and the ILR system of: (a) 15 m, (b) 20 m, (c) 25 m, and (d) 30m.

Fig. 10 shows the simulation results of the SINR change of channel 1 as a function of the laser spot duty factor under different fog conditions. As shown the SINR reduces by increasing the laser spot duty factor under the same visibilities. For high visibilities the SINR drops slowly and becoming constant, however for low visibilities the SINR drops rapidly and approaching zero for V = 50 m. As can be seen in Fig. 10, the SINR of the ILR system is strongly depend on the laser spot duty factor under different fog conditions. As can be seen for low duty factors, the laser beam (i.e., power) is more concentrated on a small spot and far away from the adjacent laser spot, thus resulting in a higher SINR. However, in this case the spacing between the adjacent laser spot is too large, which results in higher loss of target information. This research finding can be used to balance the SINR and the laser spot duty factor when designing an ILR system.

(c) The link performance considering attenuations and the inter-channel glow crosstalk:

The analysis of glow crosstalk of the ILR channel was based on the APSF for an isotropic source. The Txs used are semiconductor LD arrays with no isotropic radiation patterns. However, the target used is a standard Lambertian reflector and therefore the laser spot on the target can be considered as a first order Lambertian source where any points of the laser spot

behaves almost like an isotropic source. In the ILR system, the backscattered light received as a reflected pulse due to the fog is also significant as was investigated in our previous work [40]. Here, we ignored the backscattering effect and have focused more on the attenuation and the glow crosstalk. It is not expected to extend the glow crosstalk model to a highly directional source such as the laser spot on a specular reflected target. In such case, the accurate results of the glow crosstalk can be acquired by Monte-Carlo ray-tracing method or the numerical solution of the RTE for the specific source.

For the ILR system, the changes in the SINR of a target channel under fog is mainly due to the attenuation caused by the absorption and scattering and the inter-channel glow crosstalk, which are given by:

$$\xi_{attenuation} = 20\log_{10}\left(\frac{S_{fog}}{N_{fog}}\right) - 20\log_{10}\left(\frac{S_{clear}}{N_{clear}}\right) \text{ (dB)}, \tag{20}$$

$$\xi_{glow} = 20\log_{10}\left(\frac{S_{glow}}{N_{glow}}\right) - 20\log_{10}\left(\frac{S_{fog}}{N_{fog}}\right) \text{ (dB)}, \tag{21}$$

where S_{fog} and S_{clear}, and N_{fog} and N_{clear} are the received signal and noise voltage levels with and without fog, respectively. Note, other channels were in-active in order to avoid the influence of the inter-channel crosstalk. S_{glow} and N_{glow} are the received signal and noise voltage levels with fog, respectively and with all channels being active.

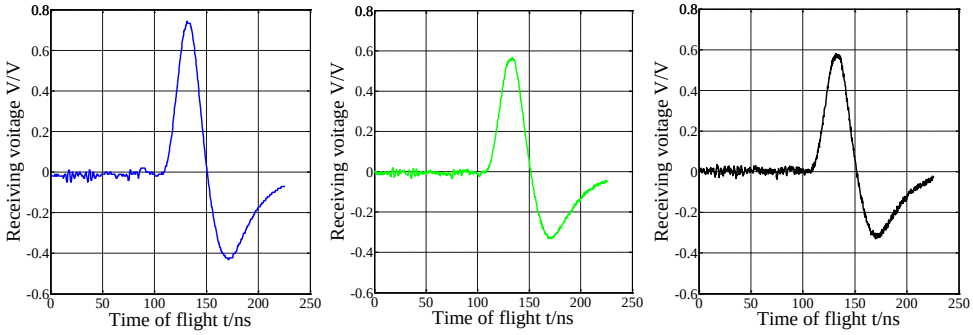

Fig. 11 The raw echo waveforms of channel 1 of ILR system of 20 m under middle fog of V = 150 m.

Fig. 11 shows the raw echo waveforms of channel 1 of ILR system of 20 m under middle fog of V = 150 m. Note that, the negative part of the signal was due to the differentiating circuit which was used to highlight the edge information of the signal. Fig. 11(a) and (b) show the received signal without and with fog and the rest channels being OFF to avoid the influence of the inter-channel crosstalk, respectively. We can see that the signal was declined due to the attenuation of fog and the noise was increased to some extent. However, Fig. 11(c) shows the received signal voltage levels with fog and with all channels operating. The influence of the inter-channel crosstalk on the signal was slight, however, the noise voltage levels increased rapidly.

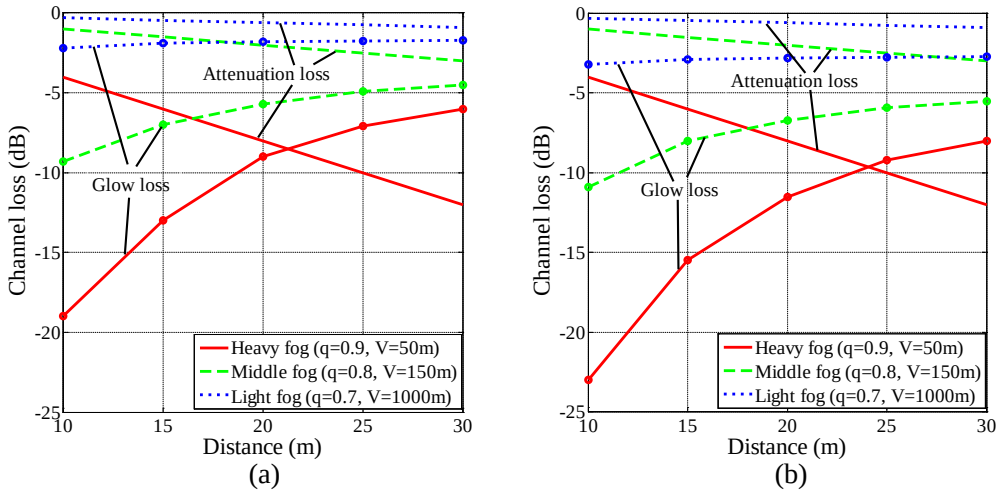

Fig.12 The channel loss due to attenuation and glow crosstalk under different fog conditions: (a) the selected channel 1, and (b) the selected channel 6.

Fig. 12 shows the channel losses as a function of the transmission span under different fog environment (i.e., light fog, middle fog and heavy fog). Figs. 12(a) and (b) are the selected c1 and c6, respectively. As can be seen, the channel loss due to the attenuation has a significant linear correlation with the ranging distance. However, the inter-channel glow crosstalk induced loss decreases with the distances. Note that, for a distance less than several tens of meters, the glow crosstalk induced loss is always large than the channel loss with no glow attenuation under light to middle fog conditions. However, under the heavy fog condition the glow crosstalk induced loss is lower for the ranging distance > 21 m. In addition, the c6 loss due to glow crosstalk is large than the c1 under the same fog environment. This is because the numbers of the effected surrounding channels of c6 are higher than c1. The results therefore illustrate that the glow crosstalk induced channel loss can be significant, which should be considered carefully when designing the ILR system and assessing its performance in the presence of fog.

4. Conclusions

In this paper, we outlined detailed theoretical analysis of the ILR system in order to determine the glow image of the light source, which was formed by the laser spot irradiated on a standard Lambertian target. Based on the theoretical model, we determined the interference due to the glow crosstalk of the adjacent channels on the typical channel. We also compared the channel loss due to the link span and the glow crosstalk under different fog conditions and showed that for a transmission distance less than several tens of meters the channel loss due to the glow crosstalk was higher than the link loss under light to medium fog conditions. However, with the dense fog and over a link span of > 21 m the link loss is higher than the glow crosstalk loss. To verify the accuracy of the proposed theoretical model, we developed a dedicated experimental setup and used it to assess the effect of fog on the 12-channels based ILR system, showing a good match between the measured and predicted SINR values under different fog conditions. The results reported can be used to optimize the design of the ILR system and analyze its performance under fog conditions.

Funding

This work is supported by funding from the National Natural Science Foundation of China (NSFC) (61371167).

Acknowledgments

This research was supported by Nanjing University of Science and Technology in China and University of Northumbria, Newcastle upon Tyne, UK. We thank the Optical Communications Research Group's Laboratory at Northumbria for the use of their test and measurement facilities.